Origin of Microstructures from Confined Asymmetric Diblock Copolymers

Peng Chen and Haojun Liang*

Hefei National Laboratory for Physical Sciences at Microscale, University of Science and Technology of China, Hefei, Anhui, 230026, People's Republic of China, and Department of Polymer Science and Engineering, University of Science and Technology of China, Hefei, Anhui, 230026, People's Republic of China

An-Chang Shi*

Department of Physics and Astronomy, McMaster University, Hamilton, Ontario L8S 4M1, Canada

Received March 1, 2007; Revised Manuscript Received July 21, 2007

ABSTRACT: The self-assembly of asymmetric diblock copolymers confined within cylindrical pores is studied using the self-consistent-field theory. The cylinder-forming asymmetric diblock copolymer is chosen to be near the cylinder−gyroid phase boundary in the intermediate segregation region. This choice makes the self-assembled cylindrical structure highly deformable, leading to very rich morphologies under confinement. A rich variety of structures, such as helices, stacked toroids, and perforated tubes, is observed as a function of the degree of confinement characterized by the ratio between the pore diameter D and bulk period L (D/L) as well as pore surface−polymer interactions. The origin of these confinement-induced structures is elucidated. The theoretical results are in good agreement with available experimental observations.

Introduction

Because of the potential of fabricating nanostructures and the desire to understand basic governing principles, the self-assembly of macromolecular systems has attracted tremendous attention in recent years. It has been shown that a rich variety of novel and complex structures can be obtained from the self-assembly (or microphase separation) of macromolecular systems containing block copolymers. Block copolymers are macromolecules composed of different subchains (blocks). From a fundamental point of view, the microphase separation of block copolymers is driven by chemical incompatibilities between the different blocks. The length scale of the self-assembled structures is dictated by the macromolecule coil size, which is on the order of 10−100 nm.[1,2]

The simplest block copolymer is a diblock copolymer, which is composed of two distinct blocks tethered together. A diblock copolymer melt can self-assemble into lamellae, cylinders, spheres, and gyroid structures depending on the chain composition and the repulsion between the different blocks.[1] More complex structures can be obtained by synthesizing more complex block copolymers, such as multiblock copolymers, or by blending different block copolymers together. Another distinct possibility to obtain new structures with existing block copolymers is to utilize geometrical confinement. When diblock copolymers self-assemble in a physically confined environment, the geometrical constraints imposed by the confinement and the interactions between the blocks and the confinement surface will play important roles in molecular organizations. It has been demonstrated that these external fields can lead to a variety of new structures.[2,3] Understanding the confined assembly of block copolymers has been an active research area in the recent years. Because of its architectural simplicity and accessibility, previous studies on the confinement effect mostly focused on thin films.[3] On the other hand, two-dimensional confining environments such as cylindrical pores are expected to produce some new phenomena. The purpose of the current study is to gain an understanding on the origin of novel structures formed from asymmetric diblock copolymers confined in cylindrical pores.

Experimentally, Xiang et al. used nanopores to physically confine a polystyrene-*b*-butadiene (PS-*b*-PBD) melt and studied confined self-assembly in cylindrical confinement.[4] Sun et al. examined the self-assembly of polystyrene-*b*-poly(methyl methacrylate) (PS-*b*-PMMA) in cylindrical channels.[5] The concentric lamellar structures observed in their experiments for symmetric diblock copolymers is consistent with earlier Monte Carlo[6,7] and dynamical density functional[8] simulations. Furthermore, experiments from Russell's group indicated the formation of novel structures such as stacked disks or toroidal-type structures in very narrow pores.[9] For diblock copolymers that form a cylindrical structure in the bulk, a helical structure is observed to form in the pores under certain conditions.[10,11] In a similar study, Wu et al. observed a series of helical structures of silica−surfactants confined within nanochannels.[12] They carried out self-consistent-field calculations to account for the observed self-assembled microstructures.

Motivated by these experiments and earlier simulations, confined self-assembly has attracted and much recent theoretical attention. Li, Wickham, and Garbary used the self-consistent mean-field theory (SCFT) to examine the two-dimensional structures of a diblock copolymer melt confined in cylindrical nanopores.[13] A systematic three-dimensional study of confined self-assembly of cylinder-forming asymmetric diblock copolymers in cylindrical pores was carried out using a simulated annealing technique by Yu et al.[14] Their results demonstrated that the confinement leads to a rich array of novel structures, many of which cannot form in the bulk. In the case of a strongly selective confinement surface, they predicted a generic morphological transition sequence, from a string of droplets to a cylinder, to helixes and then toroids. These predictions have

* To whom all correspondence should be addressed. E-mail: hjliang@ustc.edu.cn, shi@mcmaster.ca.

10.1021/ma0705164 CCC: $37.00
Published on Web 09/05/2007

been confirmed in a very recent three-dimensional SCFT study by Li and Wickham.[15] The diblock copolymers chosen by Yu et al. are close to the cylinder−sphere phase boundary in the strong segregation region. As a result of this choice, there is a very strong tendency for the block copolymers to maintain the basic cylindrical morphology. Therefore, deformations into structures other than cylinders will lead to a high-energy cost. From this point of view, the confined self-assembly studied by Yu et al. and by Li and Wickham can be regarded as a problem of optimum packing of rigid cylinders in a cylindrical pore.

In reality, the self-assembled cylinders are not rigid. This is especially true when the system is close to the cylinder−gyroid or cylinder−lamella phase boundary. The ability for the cylinders to deform will lead to more complex structures. It is of great interest to understand how this extra freedom leads to new morphologies. The purpose of the present study is to examine this interesting phenomenon. Specifically, we carried out a systematic SCFT study on cylinder-forming asymmetric diblock copolymers near the cylinder−gyroid phase region in the diblock copolymer phase diagram.[16] The self-assembled structures under different surface fields and pore diameters have been obtained. Because of the particular parameters in our system, self-assembled block copolymer cylinders can deform into perforated sheets, thereby resulting in structures which have not been observed in the copolymers studied by Yu et al. In addition to the prediction of complex structures, we attempt to elucidate the origin of these microstructures of asymmetric diblock copolymers under confinement.

Theory

An incompressible melt of diblock copolymers with a degree of polymerization N is examined in our study. Each copolymer chain is composed of two blocks (A- and B-blocks), and the volume fraction of the A-block is specified by f_A ($0 < f_A < 1$). The repulsion between the A−B monomers is characterized by a Flory−Huggins interaction parameter χ_{AB}. The bulk structures of the diblock copolymer melt are obtained using a real-space SCFT numerical scheme proposed by Drolet and Fredrickson,[17,18] with periodic boundary conditions in all three dimensions. For the structures under confinements, the diblock copolymers are confined in a cylindrical pore of diameter D and volume V (or between two planar surfaces with spacing D and volume V). For the diblock copolymer melt under confinement, the SCFT free energy per chain in the unit of k_BT has the form[19]

$$F = -\ln\left(\frac{Q}{V}\right) + \frac{1}{V}\int \mathrm{d}r[\chi_{AB}N\phi_A\phi_B - \omega_A\phi_A - \omega_B\phi_B + h_{SA}\phi_A + h_{SB}\phi_B - P(\phi_0 - \phi_A - \phi_B)] \quad (1)$$

In this expression, ϕ_A and ϕ_B are the monomer densities and $\phi_0 = \phi_A + \phi_B$ is the total monomer density. The single-chain partition function $Q = \int \mathrm{d}r\, q(r,1)$ is the partition function of a single diblock copolymer chain in the mean fields, ω_A and ω_B. These mean fields are in turn produced by the surrounding chains. The end-segment distribution function $q(r,s)$ gives the probability that a chain segment of contour length s and containing a free chain end has its "connected end" located at r. The function $q(r,s)$ and its conjugate $q'(r,s)$ satisfy the modified diffusion equations

$$\frac{\partial}{\partial s}q(r,s) = R_g^2\nabla^2 q(r,s) - N\omega q(r,s) \quad (2)$$

$$-\frac{\partial}{\partial s}q'(r,s) = R_g^2\nabla^2 q'(r,s) - N\omega q'(r,s) \quad (3)$$

with the initial conditions $q(r,0) = 1$ and $q'(r,1) = 1$. Here, R_g is the radius of gyration for an ideal Gaussian chain. For $0 \le s \le f_A$, $\omega = \omega_A$ and for $f_A < s \le 1$, $\omega = \omega_B$. We used the Crank−Nicholson scheme in solving the modified diffusion equations.

In eq 1, h_{SA} and h_{SB} represent the surface fields that the inner surface of the confinement acts on, namely, A or B monomer, respectively. P is a Lagrange multiplier (as a pressure) to ensure the incompressibility condition. Minimization of the free energy with respect to the densities and mean fields leads to the following SCFT equations:

$$\omega_A(r) = \chi_{AB}(\phi_B(r) - f_B) + h_{SA}(r) + P(r) \quad (4)$$

$$\omega_B(r) = \chi_{AB}(\phi_A(r) - f_A) + h_{SB}(r) + P(r) \quad (5)$$

$$\phi_A(r) = \frac{V}{Q}\int_0^{f_A} \mathrm{d}s\, q(r,s)\, q'(r,s) \quad (6)$$

$$\phi_B(r) = \frac{V}{Q}\int_{f_A}^{1} \mathrm{d}s\, q(r,s)\, q'(r,s) \quad (7)$$

These equations can be solved self-consistently.

Three types of confinement inner surfaces are considered in our study: (a) neutral surfaces, for which the surface has no preference to the blocks ($h_{SA} = 0$ and $h_{SB} = 0$); (b) A-attractive surface, for which the confinement surface attracts the A-blocks ($h_{SA} < 0$ and $h_{SB} = 0$); and (c) B-attractive surface, for which the confinement surface attracts the B-blocks ($h_{SA} = 0$ and $h_{SB} < 0$). For simplicity, the surface−polymer interaction potential is assumed to be short-ranged, and it is represented by contact interactions:

$$h_{SA(B)} = \begin{cases} H_{A(B)} & \text{on the lattices next to the surfaces} \\ 0 & \text{bulk} \end{cases} \quad (8)$$

where $H_{A(B)}$ is the strength of the surface field and is chosen to be -7 in this study. In order to present the fact that the polymer densities should approach zero at the confinement surface, the incompressibility condition is modified, such that $\phi_A(r) + \phi_B(r) = \phi_0(r)$, where $\phi_0(r)$ is chosen to be 0.5 on the lattices next to the surfaces and 1 everywhere else. On the surface sites of the confinement, the end-segment distribution functions and polymer densities are set to zero.

After testing several lattice sizes, we found that the free energy in the system can converge to a stable value when the lattice size is smaller than $0.3R_g$. Thus, in all calculations we took $0.2R_g$ as the lattice size. The chain contour length is divided into 200 segments.

For cylindrical confinement (the process is similar for planar confinement), the calculations are performed in cubic lattices with a circle boundary (the diameter is D) in x- and y-directions and periodic boundary conditions imposed along the axial direction of the cylindrical pore (z-direction). To obtain different pore diameters, we changed cubic lattice size in the calculation; the minimum cubic lattice size used in our calculation ($lx \times ly \times lz$) is $17 \times 17 \times lz$, and the maximum cubic lattice size used is $71 \times 71 \times lz$. To avoid the influence of periodic boundary conditions in the z-direction, the pore lengths are varied and the calculation is repeated. Each calculation is carried out starting from random homogeneous initial mean fields $\omega_{A(B)}$. We did not use any special initial conditions to obtain chiral structures in this work. All calculations are iterated until the

free energies difference between two sequential states is always less than 1.0×10^{-11}.

Under different surface fields, the pore diameters are varied to observe the self-assembled structures of an asymmetric diblock copolymer melt under cylindrical confinement. The free energies of self-assembled structures within the same pore diameter are compared to determine the stable and metastable ones. We used serial computation in this study, where the structure of the largest pore size took more than 2 weeks on an AMD Opteron 2.4G processor.

Results and Discussion

For a bulk diblock copolymer melt, the phase behavior is controlled by two parameters, f_A and $\chi_{AB}N$, which characterize the composition of the block copolymers and the degree of segregation, respectively. When the diblock copolymers are confined in a cylindrical nanopore, we expect that extra parameters such as the pore surface−polymer interactions and the pore diameter will affect the equilibrium structure. Using a simulated annealing method, Yu et al.[14] have obtained the evolution of equilibrium structures for cylinder-forming diblock copolymers confined in cylindrical channels. The diblock copolymers used in their studies have a small value of $f_A = 1/6$ or 1/4. On the bulk phase diagram, these copolymers are located in the cylindrical phase region near the cylinder−sphere phase boundary.[16] It is also believed that the model copolymers used by Yu et al. are in the strong segregation region. Because of these factors, the diblock copolymers maintain a cylinder-like structure even under confinement. Therefore, the basic ingredient in this system is the worm-like cylinders and the confinement-induced structures representing the optimum packing of these semiflexible cylinders in the confined space.

For a smaller value of $\chi_{AB}N$ and a somewhat larger value of f_A, the system is in the intermediate segregation region. In this case both theoretical and experimental studies demonstrated that a cylinder-forming system can be deformed into some other structure under planar confinement. Examples include elliptical cylinders, undulated cylinders, lamellae, undulated lamellae, and perforated lamellae.[20] It is expected that two-dimensional confinement would lead to more complex structures when the cylinders are deformed. The theoretical prediction and understanding of these confinement-induced structures are of great interest as they will lead to novel methods of fabricating nanostructures. In what follows, we report our results on the phase behavior of bulk cylinder-forming asymmetric block copolymers located near the cylinder−gyroid phase boundary. Specifically, the parameters of the diblock copolymer are $\chi_{AB}N = 14$ and $f_A = 0.36$. The pore surface−polymer interaction is specified by a parameter $H_{A(B)}$ as given in eq 8. For instance, $H_A = -7$ means that the pore surface has a preference to the A-block with a strength of 7. Such surface preference strength ($H_A = -7$) corresponds to a weak surface field, and its ratio vs segments interaction $\chi_{AB}N$ is 0.5 (7/14). However, as the following study shows, we could observe the effect of such surface preference on the block copolymers self-assembly. In a previous two-dimensional study on the phase diagram of a diblock copolymer melt confined in a cylindrical nanopore,[13] it has been demonstrated that cylinder-forming diblock copolymers located near the cylinder−gyroid phase boundary can transfer to noncylinder structures (see Figures 1 and 2 in ref 13). We believe that studying this system can lead to a deeper understanding of the physical origin for the formation of these novel structures.

1. Planar Confinement. It is noticed that systematic investigations of the phase behavior for diblock copolymers under planar confinement have already been extensively studied.[20] However, there is still no attention given to the part of the system ($f_A = 0.36$ and $\chi_{AB}N = 14$) near the cylinder−gyroid region. In the bulk, as Figure 1 shows, the system $\chi_{AB}N = 14$ and $f_A = 0.36$ form hexagonal arranged cylinders, and the equilibrium spacing between the cylinders is found to be $L = 3.7R_g$. As a reference to the two-dimensional confined systems, the structural evolution of this bulk cylinder-forming diblock copolymers under the one-dimensional (planar) confinement are presented in Figures 2, 3, and 4.

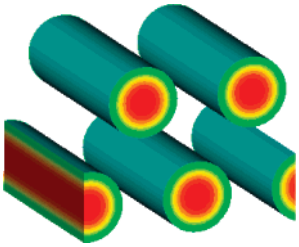

Figure 1. Self-assembled bulk cylinders structure for the system $\chi_{AB}N = 14$ and $f_A = 0.36$.

As Wang et al. [20h] show, in the case of planar confinement, the frustration of the polymer equilibrium period, which crosses two layers of cylinders ($\sqrt{3}L$), would reorient the cylinders' direction. Thus, we ordered the self-assembled structures as a function of D/L and also $D/\sqrt{3}L$. For neutral surfaces (Figure 2), the self-assembled structures maintain the cylinder-like morphology, and the same structure transition with the case of neutral surface in ref 20h is found; that is, the perpendicular cylinders arise at severe frustration conditions (such as $D/\sqrt{3}L \approx 0.25$ and 0.75, shown as Figure 2a,c) and parallel cylinders arise at loose frustration conditions (such as $D/\sqrt{3}L \approx 0.5$ and 1.0, shown as Figure 2b,d). When the planar confinement surfaces attract one of the blocks (A- or B-block), the self-assembled cylinders can deform into other structural elements, resulting in novel and more complex structures including lamellae and perforated lamellae (as Figures 3 and 4 show). In addition, the cylinders' orientations are varied from those in the neutral surface case.

Furthermore, we observed some metastable structures under planar confinement. Such structures are regular and arise at the same confinement dimension D/L. Although we could exclude the metastable structures from the stable structures by comparing the free energies, the free energies differences between those stable and metastable structures are small, and so we believe that some of the metastable structures may be observed in the experiment. To give more clues to the experimental research, these regular metastable structures are given in section I of the Supporting Information.

2. Cylindrical Confinement. For the case of two-dimensional cylindrical confinement, the phase behavior of this diblock copolymer system, $\chi_{AB}N = 14$ and $f_A = 0.36$, is more complex. Typical self-assembled structures for the three types of confining surfaces are shown in Figures 5, 6, and 7. First, we discuss the self-assembled structures when the pore surface has preference for one of the blocks.

The structural evolution in the case where the pore surface attracts the short A-blocks (that is A-attractive surface) is shown in Figure 5. As expected, the first monolayer covering the wall is the A-blocks, and the first bilayer is on the order of A−B. The structures depend critically on the diameter of the confining pores. For convenience of description, the overall morphologies can be classified in terms of the number of A-monolayers, i.e., one-layer ($D/L \leq 1.57$, shown as Figure 5a−f), two-layer (1.68

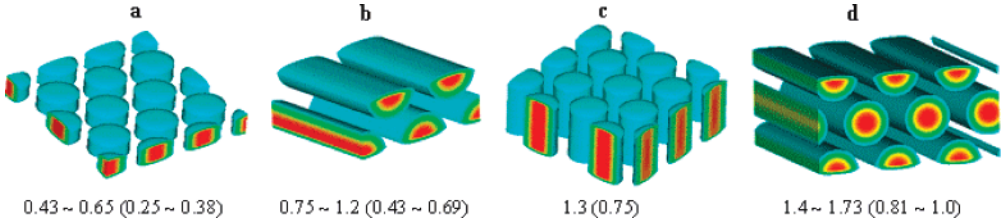

Figure 2. Self-assembled structures under planar confinement with neutral surface. The ratio of confinement spacing D vs polymer bulk period L, D/L, is shown under the typical structure, and the value of $D/\sqrt{3}L$ is shown after the D/L in the parentheses.

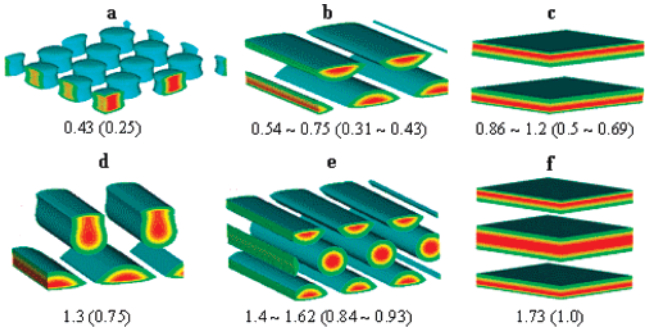

Figure 3. Self-assembled structures under planar confinement with A-attractive surface. The structures are arranged as a function of D/L (that is, the ratio of confinement spacing D vs polymer bulk period L), and the value of $D/\sqrt{3}L$ is shown after the D/L in the parentheses.

$\leq D/L \leq 3.4$, shown as Figure 5g−p), and three-layer structures ($D/L \geq 3.51$, shown as Figure 5q,r).

For a small pore with $D/L = 0.81$ (Figure 5a), there is an array of discrete droplets arranged in a zigzag-like pattern. The formation of this structure allows the system to accommodate the A-blocks in the pore by changing the size of the droplets stuck on the wall for the zigzag-like structure. For larger pores, the amount of A-blocks is increased and is enough to form cylinder-like structures. As a result, the A-blocks reassemble into double pillars ($D/L = 0.92$, Figure 5b), distorted double pillars ($D/L = 1.03$, Figure 5c), double helices ($D/L = 1.14-1.24$, Figure 5d), triple pillars ($D/L = 1.35$, Figure 5e), or four parallel pillars ($D/L = 1.46-1.57$, Figure 5f). It should be noted that the pillars and helices are both highly deformed cylinders; that is, the cross sections of these structures are flattened. These flattened cylinders can be straight, forming pillars parallel to the cylindrical pore, or they can curve up to form a helix. The one-layer structures terminate at the four parallel pillars at $D/L = 1.57$ (Figure 5f).

When the pore is large enough to produce two-layer structures, most of the A-blocks are initially consumed by four outside parallel pillars ($D/L = 1.68$, Figure 5g). Because forming pillars with very large cross sections will lead to a high-energy structure, the remaining A-blocks are pushed to the center of the pore. At the very beginning, the amount of the excess A-blocks is not sufficient to form a cylinder in the center. Therefore, they assemble into a set of discrete droplets. For a larger pore diameter ($D/L = 1.78-1.89$), the amount of A-blocks increases so that the string of droplets transforms into a cylinder at the center of the pore (Figure 5h). A further increase of the pore diameter leads to a structure with an inner cylinder and an outer perforated tube ($D/L = 2.0-2.43$, Figure 5i). Two-layer structures terminate at a double-perforated tube at $D/L = 3.4$, wherein both the outer and inner layers are perforated tubes. The perforated tubes are similar to the perforated lamellae observed in the one-dimensional confinement (Figure 4c,g). Specifically, these perforated tubes may be regarded as folded perforated lamella formed in one-dimensional planar confinement. Although the overall structures of the block copolymers maintain a two-layer form, the morphology is very complex, as can be seen in Figure 5. The outside layer can assume a range of morphologies including four pillars, a perforated tube, a stack of toroids, and a helix. At the same time, the inner layer can be a string of droplets, a straight cylinder, a stack of disks, a single helix, double helices, and a perforated tube.

In particular, a novel structure with outside stacked toroids and inner stacked disks is predicted at $D/L = 2.54$ (Figure 5j). The formation of this inner stacked disks structure may be related to the incommensurateness of pore diameter D with polymer period L. As Figures 2, 3, and 4 show, under planar confinement, when the structure frustration is severe (for those $D/L \approx 0.25$ or 0.75), the cylinders would orient perpendicularly to the confined surface to retain the bulk period. This should be same with the cylindrical confinement case, where at severe frustration the cylinder may orient perpendicularly to the pore wall. Owing to the curvature of the confined geometry in the cylindrical confinement, the cylinders should be bent along the latitudinal line of the pore. Finally, they form a toroid as long as the confined space is closed. The inner stacked disks may still be regarded as the stacked toroids, which appear as stacked-disk-like because of the inner connection of the toroids in a very small size pore. This point becomes clearer at a larger size pore at $D/L = 3.51$ (Figure 5q), in which the intermediate layers appear in the stacked-toroid-like structure. At the outside layer, there are stacked toroids at $D/L = 2.54$ (Figure 5j) and 3.51 (Figure 5q), which may be formed to relieve the nonuniform chain stretching between the interior disks or toroids. Previous studies (refs 14 and 15) also observed the inner stacked disks following the cylinder structures region and stacked toroids following the helix structures region. However, the outside toroid structures presumably do not form in these studies[14,15] due to the high-energy penalty for deforming the cross section of the cylinders when they are near the wall. Because our system is easily deformable, the energy penalty is less, which facilitates the formation of outside toroid structures.

Further increasing the pore size leads to a transition from two-layer structures to three-layer structures. The initial stage for the formation of this third layer is a transition from a string of droplets ($D/L = 3.51$, Figure 5q) to a cylinder in the center of the pore ($D/L = 3.73$, Figure 5r), closely resembling those in the second layer ($D/L = 1.68-2.0$, Figure 5g−i). The largest pore used in our calculations is $D/L = 3.73$. Further calculations in a larger pore are beyond our computational capability. However, we can reasonably expect that the third inner layer might terminate at a perforated tube after experiencing a variety of transitions from a cylinder to a helix, to a double helix, to stacked toroids, repeating the sequence in the formation of the second layer.

In fact, both previous[14,15] and present studies show a "typical" structural evolution sequence for the interior structures under cylindrical confinement, that is, from discrete droplets (sphere-like), to one cylinder, stacked disks, and finally a helix with

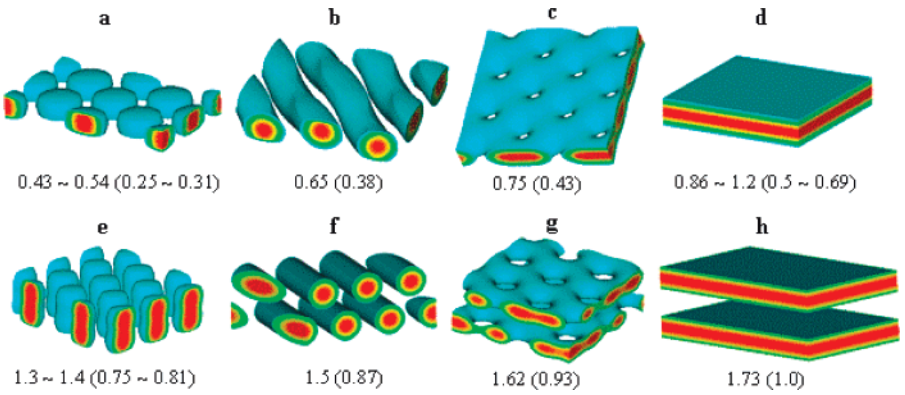

Figure 4. Self-assembled structures under planar confinement with B-attractive surface. The structures are arranged as a function of D/L (that is, the ratio of confinement spacing D vs polymer bulk period L), and the value of $D/\sqrt{3}L$ is shown after the D/L in the parentheses.

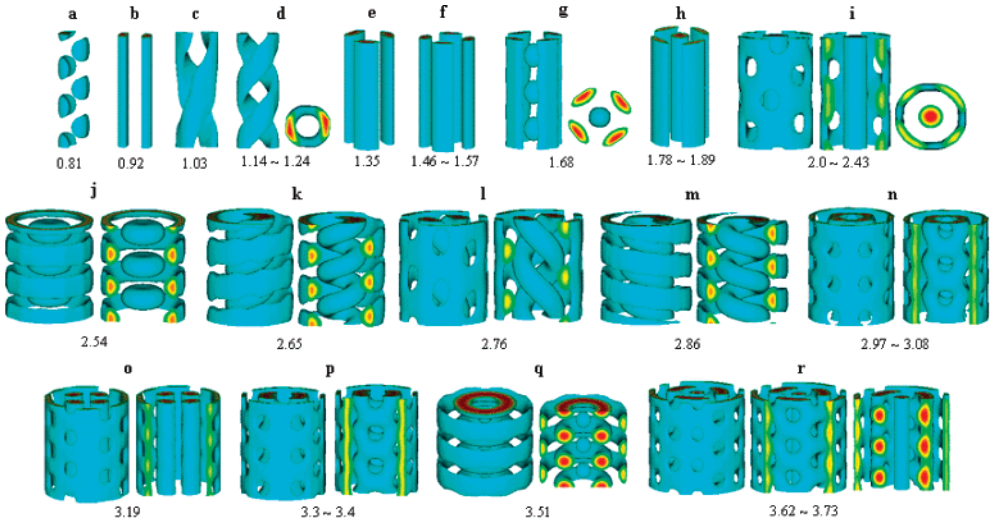

Figure 5. Self-assembled structures under cylindrical confinement with A-attractive surface. The structures are arranged as a function of D/L (that is, the ratio of pore diameter D vs polymer bulk period L), and some top views (d, g, i) and cut views (i−r, that is $D/L \geq 2.0$) are shown for clarity.

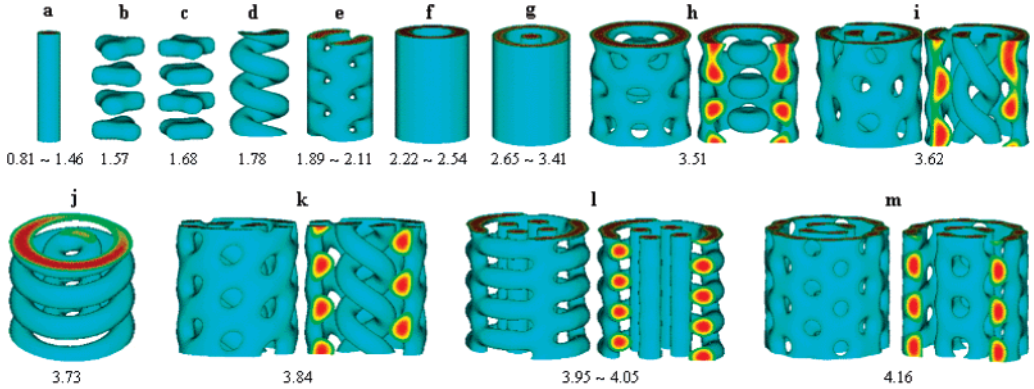

Figure 6. Self-assembled structures under cylindrical confinement with B-attractive surface. The structures are arranged as a function of D/L (that is, the ratio of pore diameter D vs polymer bulk period L), and some cut views (h, i, k, l, m) are shown for clarity.

the pore diameter increasing. Such a transition may be ascribed to the increase in material amount at the pore center, which is common for all diblock copolymers systems.

Some regular metastable structures are also observed under cylindrical confinement (see section II of the Supporting Information). An interesting observation is that most metastable structures appear when D is incommensurate with L (e.g., $D/L \approx 2.5, 3.5$), whereas in most cases, only one equilibrium structure is obtained when D is commensurate with L (e.g., $D/L \approx 2.0, 3.0$). This phenomenon originates from the fact that for the commensurate cases the geometrical confinement does not lead to severe structural frustration; thus, the stable structure can form naturally. On the other hand, the incommensurate case leads to severe structural frustrations and results in a complex free energy landscape with many local minima having similar free energies. The regular metastable structures were generally obtained via changing the random mean fields at the initial stage in calculation. We expect that these structures could be experimentally realized with small controlled variation of experimental conditions such as local density fluctuations, sample inhomogeneities, and temperature fluctuations.

When the pore surface attracts the long blocks (B-block) by taking $H_B = -7$ in eq 8 (that is B-attractive surface), the B-blocks are attracted to the surfaces, leading to a first bilayer

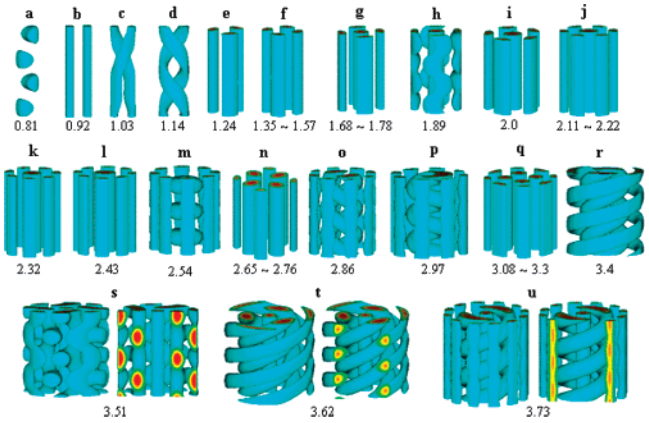

Figure 7. Self-assembled structures under cylindrical confinement with neutral surface. The structures are arranged as a function of D/L (that is, the ratio of pore diameter D vs polymer bulk period L), and some cut views (s, t, and u, that is $D/L \geq 3.51$) are shown for clarity.

close to the surface in a B−A order. It has been demonstrated that the B-attractive surface can produce similar structures as those in A-attractive surface pores at the effective pore diameter.[14,15] As displayed in Figure 6, the first A-blocks structure (a cylinder) at $D/L = 0.81-1.46$ (Figure 6a) is exactly identical to the inner A-blocks structure at $D/L = 2.0-2.43$ (Figure 5i) after neglecting the outside A-blocks domain in Figure 5 (A-attractive surface), which is in accordance with previous studies.[14,15] Further increasing the pore size produces stacked disks (triangle-like: $D/L = 1.57$; square-like: $D/L = 1.68$), a helix ($D/L = 1.78$), and then a perforated tube at $D/L = 1.89-2.11$ (Figure 6b−e). This structural evolution resembles that of A-attractive surface pores in the range of $D/L = 2.0-3.08$ (Figure 5i−n). However, the outside tube structures (the curved lamellae) arise at the B-attractive cases for $D/L = 2.22-3.41$ (Figure 6f,g), which is not observed in the A-attractive surface case. The difference between the structures generated in these two types of pores can be ascribed to the fact that the studied system is highly deformable, which makes the correspondence of the A-attractive surface case with the B-attractive surface case not as strong as previous studies.[14,15] Moreover, in the B-attractive surface case, the stacked disks arise at the severe incommensurate conditions that is $D/L = 1.57-1.68$, 3.51 (Figure 6b,c,h), and the parallel cylinder structures (the inner layer for multiple layers structures) arise at the commensurate conditions that is $D/L \approx 1.0$, 3.0, and 4.0 (Figure 6a,g,l), considering that the outside structures at $D/L \approx 3.0$ and 4.0 (Figure 6g,l) are highly deformed by the surface interaction.

It was mentioned earlier that, although we are unable to perform calculations for larger A-attractive surface pores with $D/L > 3.73$, we could extrapolate the results for smaller pores to predict that the third A-monolayer should terminate at a perforated tube after experiencing a series of intermediate structures (such as single helix, double helices, and stacked toroids). This prediction is verified by observing the formation of the second A-blocks structures in the case of the B-attractive surface. We indeed observed these intermediate structures, namely, single helix, double helices, and stacked toroids, in the pores with $D/L > 3.41$, and finally, a perforated tube at $D/L = 4.16$ (Figure 6m), in agreement with our expectation. All observed structures including stable and metastable ones in the B-attractive surface cases are listed in section II of the Supporting Information.

We now turn our attention to the case of neutral pores. For this particular condition, all the assembled structures by the A-blocks, both in the bulk and under the neutral planar confinement, are cylinders or pillars (Figures 1 and 2). It would be very interesting to understand what will occur under cylindrical confinement. Typical structures formed by the A-blocks in the neutral pores are summarized in Figure 7.

During severe confinement in the small pores with $D/L \leq 0.81$, the polymer chains are severely frustrated, hence resulting in a string of discrete droplets (Figure 7a). For some larger pores, two parallel pillars ($D/L = 0.92$, Figure 7b) or two distorted pillars ($D/L = 1.03$, Figure 7c) and a helix structure ($D/L = 1.14$, Figure 7d) are formed. Such monolayer structures ended at $D/L = 1.57$ (Figure 7f), and the most self-assembled structures are pillar-like, resembling those produced in the bulk or under neutral planar confinement. For $1.68 \leq D/L \leq 2.43$ (Figure 7g−l), the second layer structures formed, most of which are the complex of outside pillars and inner cylinders except for $D/L = 1.89$ (Figure 7h), in which the outside pillars are undulated. For $D/L = 2.54$ (Figure 7m), which is the severe frustration condition, the inner layer are stacked circle disks. For $D/L = 2.65-2.76$ (Figure 7n), the interface between the outside and the inner layers disappeared; that is, the deformed cylinders stretched across the outside layer and the inner layer, which implies a change would occur for interior structures. Next, we observed the inner helix structures at $D/L = 2.86-2.97$ (Figure 7o,p), despite the outside structure close to the wall being pillar-like. After that, the system is retrieved to be a complex of outside pillars and inner cylinders ($D/L = 3.08-3.3$, Figure 7q).

It seems that the helix structures at $D/L = 2.86$ and 2.97 (Figure 7o,p) are the adjustment of inner cylinders. That is, as the inner material increases but is still not suitable to form more evenly dispersed cylinders, it may employ a distorted form with a larger cross-section like a helix to consume more material in the pore center. This is the same for the inner helix structures in larger pore diameter cases ($D/L = 3.4$, 3.62, and 3.73: shown as Figure 7r,t,u). The formation mechanism of helix structures under A- or B-attractive surface cases should also be the same with that in the neutral surface case. However, the pore diameters regions for the formation of helix structures vary from each other under different surface field cases. Furthermore, at A- or B-attractive surface cases, the outside layers could be reconstructed to be a perforated tube for the system of $\chi_{AB}N = 14$ and $f_A = 0.36$ due to the surface preference to one of the blocks. In comparison, under the neutral surface field, the outside layers remain pillar-like. However, in some cases, the outside pillar structures may be distorted to be a helix ($D/L = 3.4$, 3.62: shown as Figure 7r,t) or undulated pillars ($D/L = 1.89$ and 3.51: shown as Figure 7h,s) to relieve the interior structures stretching. In the neutral surface case, the perforated tubes are only observed in the inner layers of some metastable structures (Supporting Information: section II).

Being similar to A- or B-attractive surfaces cases, under the neutral surface, when frustration is weak (D/L is close to an integer, such as 2.0 and 3.0), the cylinders orient parallel to the cylindrical pore, and when frustration is severe (D/L is close to a half integer), the A-blocks domain is inclined to orient perpendicularly to the pore surface. For instance, when $D/L = 2.54$ (Figure 7m), the inner layer is stacked disks. For $D/L = 3.51$ (Figure 7s), although we did not observe perpendicular cylinders as that in ref 14 (Figure 1c, $D/L = 3.5$), the intermediate layer structure is irregular, and parts of it protuberate perpendicular to the pore surface, which indicates that the polymer system undergoes severe frustration.

3. Comparison with Other Simulations and Experiments. There are two major differences between this study and previous studies.[14,15] One is the perforated tube structure that is not

observed in previous studies.[14,15] This may be ascribed to the easy deformability of the system $\chi_{AB}N = 14$ and $f_A = 0.36$, and the surface preference for one of the blocks seems necessary for the formation of the outside perforated tube. The other is the outside layer structures, in the case where pore surface attracts short blocks (A-attractive surface in this study). Previous studies presumably did not observe regular outside layer structures. Meanwhile, in our system, the outside layer structures form as a result of relieving interior structures stretching. At the same time, previous and present studies all show the "typical" structural transition sequence; that is, the interior structures in the pore vary from discrete droplets (sphere-like), to one cylinder, stacked disks, and a helix with the pore diameter increasing.

Xiang et al. experimentally investigated the self-assembly of asymmetric PS-*b*-PBD within the alumina cylindrical pore having the PBD-attractive wall,[4,10,11] for which the shorter BD-blocks (the volume fraction of PBD is 0.36) form hexagonal cylinders in the bulk, resembling the system with $H_A = -7$ which we used in the calculation. They observed helical structures in pores $D/L = 1.1-1.5$ (see Figure 3F,G in ref 11). This observation is in accordance with our calculation in the range of $D/L = 1.03-1.24$ (Figure 5c,d). For pores with diameters in the range of $D/L = 1.9-2.3$, a single cylinder comprised of PBD blocks is located in the center of the nanopore (see Figure 3D,E in ref 11). The cross-sectional view along the pore shows some undulations along the PBD layer that is located close to the wall (Figure 3E in ref 11). This implies that the outside PBD layer close to the wall is not constructed by a solid tube. In comparison with our calculation, corresponding to the pore having diameters in the range of $D/L = 2.0-2.43$ as in Figure 5i, there is a two-layer structure with a cylinder at the center and a perforated tube at the wall. [The cross-sectional view along the pore in our calculation displays a similar undulation to the experimental observation (Figure 3E in ref 11) along the rim of the outside layer, and the view across the pore is exactly the same as that of the experimental one (Figure 3D in ref 11).] Therefore, we infer that the experimentally observed outside layer corresponding to $D/L = 1.9-2.3$ (Figure 3D,E in ref 11) might be a perforated tube, resembling that of our calculation in the range of $D/L = 2.0-2.43$ (Figure 5i).

Conclusion

The self-assembly of asymmetric diblock copolymer within cylindrical confinement has been explored using the SCFT calculation. By choosing the chain parameters $\chi_{AB}N = 14$ and $f_A = 0.36$, a rich variety of structures was observed, most of which have not been observed previously. A good agreement between the experiment's observation and our calculation was found. We explain the origin of these microstructures in relation to the confinement dimension D/L. When the confinement diameter D is commensurate with polymer period L, the system could readily reach a local free energy minimum under the compromise of surface preference and accommodation with confined pore diameter. The frustration constrained by the confinement at the incommensurate case may lead the system into the complex free energy landscape state. Furthermore, the severe confinement frustration tends to orientate structures perpendicularly to the pore surface. Our study shows that the system at relative weak segregation is easily deformable under cylindrical confinement, and its phase behavior is more complex than the rigid system, which may be used to fabricate more subtle materials in nanoscale.

Acknowledgment. We are grateful for the financial support provided by the Outstanding Youth Fund (No. 20525416), the Programs of the National Natural Science Foundation of China (Nos. 20490220, 20374050, and 90403022), and the National Basic Research Program of China (No. 2005CB623800). ACS is supported by the Natural Sciences and Engineering Council (NSERC) of Canada. ACS gratefully acknowledges the hospitality of Profs. Chi Wu, Haojun Liang, Shiyong Liu, Guangzhao Zhang, and the Hefei National Laboratory for Physical Sciences at Microscale, where the work was carried out when he was a visiting professor. Parts of the calculations were carried out at the Shanghai Supercomputer Center.

Supporting Information Available: All observed structures under planar confinement and cylindrical confinement. This material is available free of charge via the Internet at http://pubs.acs.org.

References and Notes

(1) Bates, F. S.; Fredrickson, G. H. *Phys. Today* **1999**, *52*, 32.
(2) Pereira, G. G. *Curr. Appl. Phys.* **2004**, *4*, 255.
(3) (a) Lambooy, P.; Russell, T. P.; Kellogg, G. J.; Mayes, A. M.; Gallagher, P. D.; Satija, S. K. *Phys. Rev. Lett.* **1994**, *72*, 2899. (b) Masten, M. W. *J. Chem. Phys.* **1997**, *106*, 7781. (c) Geisinger, T.; Muller, M.; Binder, K. *J. Chem. Phys.* **1999**, *111*, 5241. (d) Geisinger, T.; Muller, M.; Binder, K. *J. Chem. Phys.* **1999**, *111*, 5251. (e) Wang, Q.; Nealey, P. F.; de Pablo, J. J. *Macromolecules* **2001**, *34*, 3458. (f) Huimink, H. P.; Brokken-zijp, J. C. M.; van Dijk, M. A.; Sevink, G. J. A. *J. Chem. Phys.* **2000**, *112*, 2452. (g) Xu, T.; Hawker, C. J.; Russell, T. P. *Macromolecules* **2005**, *38*, 2802. (h) Tsarkova, L.; Knoll, A.; Krausch, G.; Magerle, R. *Macromolecules* **2006**, *39*, 3608.
(4) Xiang, H.; Shin, K.; Kim, T.; Moon, S. I.; McCarthy, T. J.; Russell, T. P. *Macromolecules* **2004**, *37*, 3660.
(5) Sun, Y.; Steinhart, M.; Zschech, D.; Adhikari, R.; Michler, G. H.; Gosele, U. *Macromol. Rapid Commun.* **2005**, *26*, 369.
(6) He, X. H.; Song, M.; Liang, H. J.; Pan, C. Y. *J. Chem. Phys.* **2001**, *114*, 10510.
(7) Chen, P.; He, X. H.; Liang, H. J. *J. Chem. Phys.* **2006**, *124*, 104906.
(8) Sevink, G. J. A.; Zvelindovsky, A. V.; Fraaije, J. G. E. M.; Huinink, H. P. *J. Chem. Phys.* **2001**, *115*, 8226.
(9) Shin, K.; Xiang, H.; Moon, S. I.; Kim, T.; McCarthy, T. J.; Russell, T. P. *Science* **2004**, *306*, 76.
(10) Xiang, H.; Shin, K.; Kim, T.; Moon, S. I.; McCarthy, T. J.; Russell, T. P. *Macromolecules* **2005**, *38*, 1055.
(11) Xiang, H.; Shin, K.; Kim, T.; Moon, S.; Mccarthy, T. J.; Russell, T. P. *J. Polym. Sci., Part B: Polym. Phys.* **2005**, *43*, 3377.
(12) Wu, Y.; Cheng, G.; Katsov, K.; Sides, S. W.; Wang, J.; Tang, J.; Fredrickson, G. H.; Moskovits, M.; Stucky, G. D. *Nat. Mater.* **2004**, *3*, 816.
(13) Li, W.; Wickham, R. A.; Garbary, R. A. *Macromolecules* **2006**, *39*, 806.
(14) Yu, B.; Sun, P.; Chen, T.; Jin, Q.; Ding, D.; Li, B.; Shi, A.-C. *Phys. Rev. Lett.* **2006**, *96*, 138306.
(15) Li. W.; Wickham, R. A. *Macromolecules* **2006**, *39*, 8492.
(16) Matsen, M. W.; Bates, F. S. *Macromolecules* **1996**, *29*, 1091.
(17) Drolet, F.; Fredrickson, G. H. *Phys. Rev. Lett.* **1999**, *83*, 4317.
(18) Drolet, F.; Fredrickson, G. H. *Macromolecules* **2001**, *34*, 5317.
(19) Chen, H-Y.; Fredrickson, G. H. *J. Chem. Phys.* **2002**, *116*, 1137.
(20) (a) Turner, M. S.; Rubinstein, M.; Marques, C. M. *Macromolecules* **1994**, *27*, 4986. (b) Krausch, G.; Magerle, R. *Adv. Mater.* **2002**, *14*, 1579. (c) Pereira, G. G. *J. Chem. Phys.* **2002**, *117*, 1178. (d) Huimink, H. P.; van Dijk, M. A.; Brokken-zijp, J. C. M.; Sevink, G. J. A. *Macromolecules* **2001**, *34*, 5325. (e) Park, I.; Park, S.; Park, H. W.; Chang, T. *Macromolecules* **2006**, *39*, 315. (f) Tsarkova, L.; Knoll, A.; Krausch, G.; Magerle, R. *Macromolecules* **2006**, *39*, 3608. (g) Yang, Y.; Qiu, F.; Zhang, H.; Yang, Y. *Polymer* **2006**, *47*, 2205. (h) Wang, Q.; Nealey, P. F.; de Pablo, J. J. *Macromolecules* **2001**, *34*, 3458.

MA0705164